

# Ultrathin Amorphous/Crystalline Heterophase Rh and Rh Alloy Nanosheets as Tandem Catalysts for Direct Indole Synthesis

Jingjie Ge, Peiqun Yin, Ye Chen, Hongfei Cheng, Jiawei Liu, Bo Chen, Chaoliang Tan, Peng-Fei Yin, Hong-Xing Zheng, Qiang-Qiang Li, Shuangming Chen, Wenjie Xu, Xiaoqian Wang, Geng Wu, Rongbo Sun, Xiang-Huan Shan, Xun Hong, and Hua Zhang\*

Heterogeneous noble-metal-based catalysis plays an essential role in the production of fine chemicals. Rh-based catalysts are one of the most active candidates for indole synthesis. However, it is still highly desired to develop heterogeneous Rh-based catalysts with high activity and selectivity. In this work, a general, facile wet-chemical method is reported to synthesize ultrathin amorphous/crystalline heterophase Rh and Rh-based bimetallic alloy nanosheets (NSs), including RhCu, RhZn, and RhRu. Impressively, the amorphous/crystalline heterophase Rh NSs exhibit enhanced catalytic activity toward the direct synthesis of indole compared to the crystalline counterpart. Importantly, the obtained amorphous/crystalline heterophase RhCu alloy NSs can further enhance the selectivity to indole of >99.9% and the conversion is 100%. This work demonstrates the importance of phase engineering and metal alloying in the rational design and synthesis of tandem heterogeneous catalysts toward fine chemical synthesis.


Owing to the preeminent heterocyclic motifs, indoles exhibit excellent biological activity in chemical industry and life science, such as pharmaceuticals, agrochemicals, and fragrances.<sup>[1,2]</sup> One of the most efficient and cost-effective methods to produce indoles is the direct synthesis via the tandem reaction,<sup>[3–6]</sup> i.e., the condensation between aniline reduced from nitroarene and its adjacent aldehyde group. Importantly, Rh-based catalysts are among the most active catalysts for the indoles synthesis.<sup>[7–9]</sup> Particularly, heterogeneous Rh-based catalysts are promising candidates owing to their stability, recyclability, and facile segregation.<sup>[10,11]</sup> However, they still suffer from the low catalytic activity and selectivity compared to the homogeneous

Dr. J. Ge, Dr. P. Yin, Dr. Y. Chen, Dr. H. Cheng, J. Liu  
Center for Programmable Materials  
School of Materials Science and Engineering  
Nanyang Technological University  
50 Nanyang Avenue, Singapore 639798, Singapore  
Dr. P. Yin, Dr. X. Wang, Dr. G. Wu, R. Sun, Prof. X. Hong  
Center of Advanced Nanocatalysis (CAN)  
Hefei National Laboratory for Physical Sciences at the Microscale  
University of Science and Technology of China  
Hefei, Anhui 230026, China

Dr. P. Yin  
School of Chemistry and Environmental Engineering  
Institute of Low-dimensional Materials Genome Initiative  
Shenzhen University  
Shenzhen 518060, China

Dr. Y. Chen  
Department of Chemistry  
The Chinese University of Hong Kong  
Shatin, N.T., Hong Kong, China

Dr. B. Chen, Dr. P.-F. Yin, Prof. H. Zhang  
Department of Chemistry  
City University of Hong Kong  
Hong Kong, China  
E-mail: Hua.Zhang@cityu.edu.hk

 The ORCID identification number(s) for the author(s) of this article can be found under <https://doi.org/10.1002/adma.202006711>.

Dr. C. Tan  
Department of Electrical Engineering  
City University of Hong Kong  
Hong Kong, China

Dr. H.-X. Zheng  
School of Chemistry and Chemical Engineering  
Liaocheng University  
Liaocheng, Shandong 252059, China

Dr. Q.-Q. Li  
School of Physical and Mathematical Sciences  
Nanyang Technological University  
21 Nanyang Link, Singapore 637371, Singapore

Dr. S. Chen, W. Xu  
National Synchrotron Radiation Laboratory  
CAS Center for Excellence in Nanoscience  
University of Science and Technology of China  
Hefei, Anhui 230029, China

Dr. X.-H. Shan  
Department of Chemistry  
University of Science and Technology of China  
Hefei, Anhui 230026, China

Prof. H. Zhang  
Hong Kong Branch of National Precious Metals Material  
Engineering Research Center (NPMM)  
City University of Hong Kong  
Hong Kong, China

DOI: 10.1002/adma.202006711

catalysts.<sup>[12–15]</sup> Therefore, it is highly desired to develop efficient Rh-based heterogeneous catalysts for the indole synthesis.

Developing facile synthetic methods for synthesis of noble metal nanocatalysts has attracted great attention.<sup>[11,16]</sup> Recent studies on phase engineering of nanomaterials (PEN)<sup>[17]</sup> have revealed the crucial role of phases in determining the properties, functions, and applications of noble metal heterogeneous nanocatalysts. As one of important groups of materials in the field of PEN, heterophase nanomaterials comprising of more than one phases in individual nanostructures have demonstrated tremendous potentials in catalysis,<sup>[18–22]</sup> owing to the synergistic effect between different phases and the abundant active sites at the phase boundaries and/or interfaces.<sup>[23,24]</sup> For example, amorphous/crystalline heterophase Pd-based nanosheets (NSs) demonstrate better chemoselectivity than their crystalline counterpart toward the selective hydrogenation of C=C bond in 4-nitrostyrene.<sup>[23,25]</sup> Furthermore, alloying noble metal catalysts with non-precious metals can reduce the cost and might also improve the catalytic performance due to the synergistic effects between different metal components.<sup>[26–28]</sup> For instance, the catalytic activity and selectivity of Ru catalysts toward the hydrogenation of 4-nitrostyrene<sup>[29]</sup> and electrocatalytic hydrogen evolution<sup>[30]</sup> can be efficiently boosted by introducing Co atoms and regulating their lattice strain. However, to the best of our knowledge, the synthesis of heterophase Rh and Rh-based alloyed nanomaterials has not been

realized, hindering the exploration of their performances as tandem catalysts.

Here, we report a surfactant-free, one-pot synthesis of ultrathin Rh NSs with amorphous/crystalline heterophase (denoted as *a/c*-Rh NSs). The crystallinity of Rh NSs can be tuned by controlling the reaction temperature. Our general method is also applicable to synthesize Rh-based bimetallic alloy NSs with amorphous/crystalline heterophase, e.g., RhCu, RhZn, and RhRu. As a proof-of-concept application, when used as tandem catalyst for the direct synthesis of indole, the amorphous/crystalline heterophase Rh NSs outperform their crystalline counterpart with much higher catalytic activity toward the indole production. Impressively, via further Cu alloying, the amorphous/crystalline heterophase RhCu NSs demonstrate significantly enhanced indole selectivity of over 99.9% with high activity.

The *a/c*-Rh NSs are prepared by reducing the Rh(acac)<sub>3</sub> in a diluted aqueous formaldehyde solution without any surfactant in an autoclave at a mild temperature (90 °C) for 18 h (see the Experimental Section in the Supporting Information for experimental details). The Rh nanostructure with a sheet-assembled flower-like morphology is obtained in high yield, which was confirmed by the scanning electron microscopy (SEM) (Figure 1a) and dark-field scanning transmission electron microscopy (DF-STEM) images (Figure 1b). The formation of flower-like morphology is likely due to the

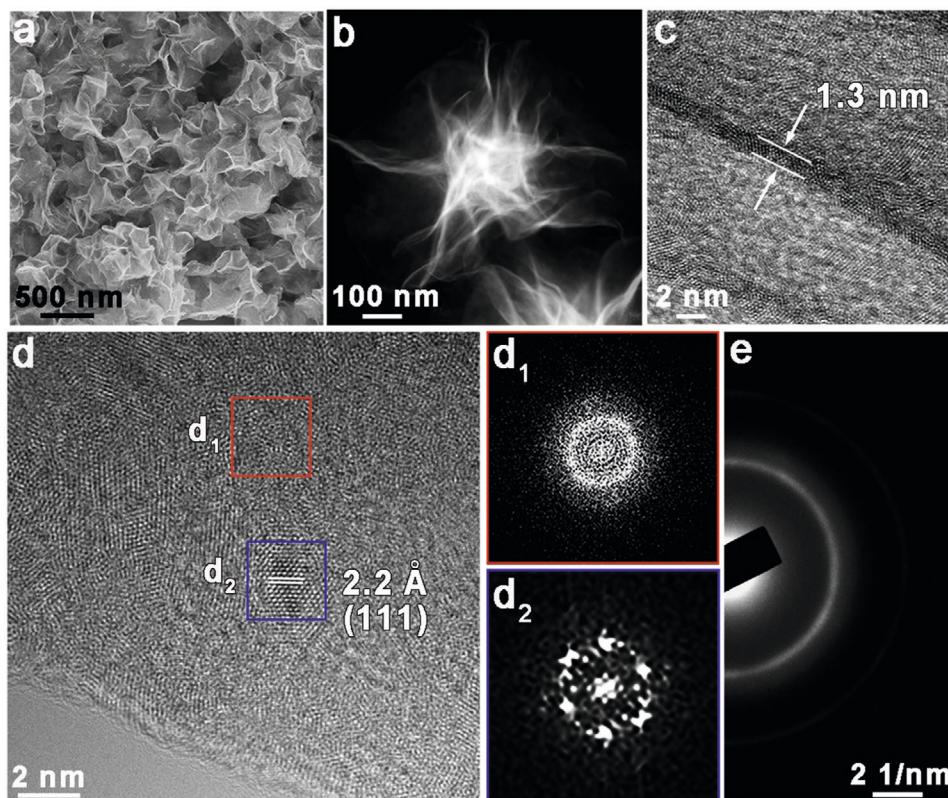


**Figure 1.** Characterization of the synthesized *a/c*-Rh NSs. a) SEM and b) DF-STEM images of Rh NSs. c) TEM image of a typical folded Rh NS, showing the thickness of  $\approx 1.3$  nm. d) A typical aberration-corrected HRTEM image showing the heterophase structure, in which the representative amorphous and crystalline domains are marked by the red and blue squares, respectively.  $d_1, d_2$ ) FFT patterns taken from the red and blue squares in (d), respectively. e) SAED pattern of the *a/c*-Rh NSs.

presence of formaldehyde in the hydrothermal synthesis.<sup>[31]</sup> The average thickness of the NSs was measured to be about 1.3 nm (Figure 1c; Figure S1, Supporting Information). Aberration-corrected high-resolution transmission electron microscopy (HRTEM) was utilized to investigate the NSs at the atomic scale. As illustrated in Figure 1d, a typical Rh NS consists of many amorphous and crystalline domains. In a representative amorphous region ( $d_1$ , red square area), Rh atoms are arranged without obvious long-range order. In a representative crystalline region ( $d_2$ , blue square area), the crystal lattice with a lattice spacing of 2.2 Å is measured, corresponding to the (111) plane of face-centered cubic (fcc) Rh.<sup>[32]</sup> The diffuse ring (Figure 1d<sub>1</sub>) and the bright spots (Figure 1d<sub>2</sub>) in the corresponding selected-area fast Fourier transform (FFT) patterns illustrate the amorphous and crystalline phases in the Rh NSs, respectively. Different from the crystalline Rh NSs (denoted as *c*-Rh NSs, Figure S2, Supporting Information) which were obtained under the same reaction condition except that the reduction temperature was changed to 170 °C (see the Experimental Section in the Supporting Information for experimental

details), the *a/c*-Rh NSs possess many amorphous–crystalline phase boundaries (Figure S3, Supporting Information). Moreover, the low degree of crystallinity in *a/c*-Rh NSs is reflected by the weak diffraction ring in the selected area electron diffraction (SAED) pattern (Figure 1e). The X-ray diffraction (XRD) pattern of the *a/c*-Rh NSs (Figure S4, Supporting Information) shows one weak and broad peak at 41.0° ascribed to the diffraction from the fcc Rh (111) plane, which also indicates the poor crystallinity of the *a/c*-Rh NSs. The formation of *a/c*-Rh NSs at lower reaction temperature (90 °C) compared to that of *c*-Rh NSs (170 °C) is similar to the previous studies on the *a/c*-Pd and *a/c*-PdCu NSs.<sup>[23,25]</sup>

The chemical state of Rh was confirmed by X-ray photoelectron spectroscopy (XPS). As shown in Figure 2a, the binding energy peaks of *a/c*-Rh NSs at 307.5 and 312.2 eV can be assigned to Rh 3d<sub>5/2</sub> and Rh 3d<sub>3/2</sub> of metallic Rh(0), respectively. Compared to the *c*-Rh NSs (307.2 and 311.9 eV), the Rh 3d peaks of the *a/c*-Rh NSs slightly shift to higher binding energy, which could be attributed to the atomic disordering in the amorphous phase.<sup>[33,34]</sup> Moreover, X-ray absorption

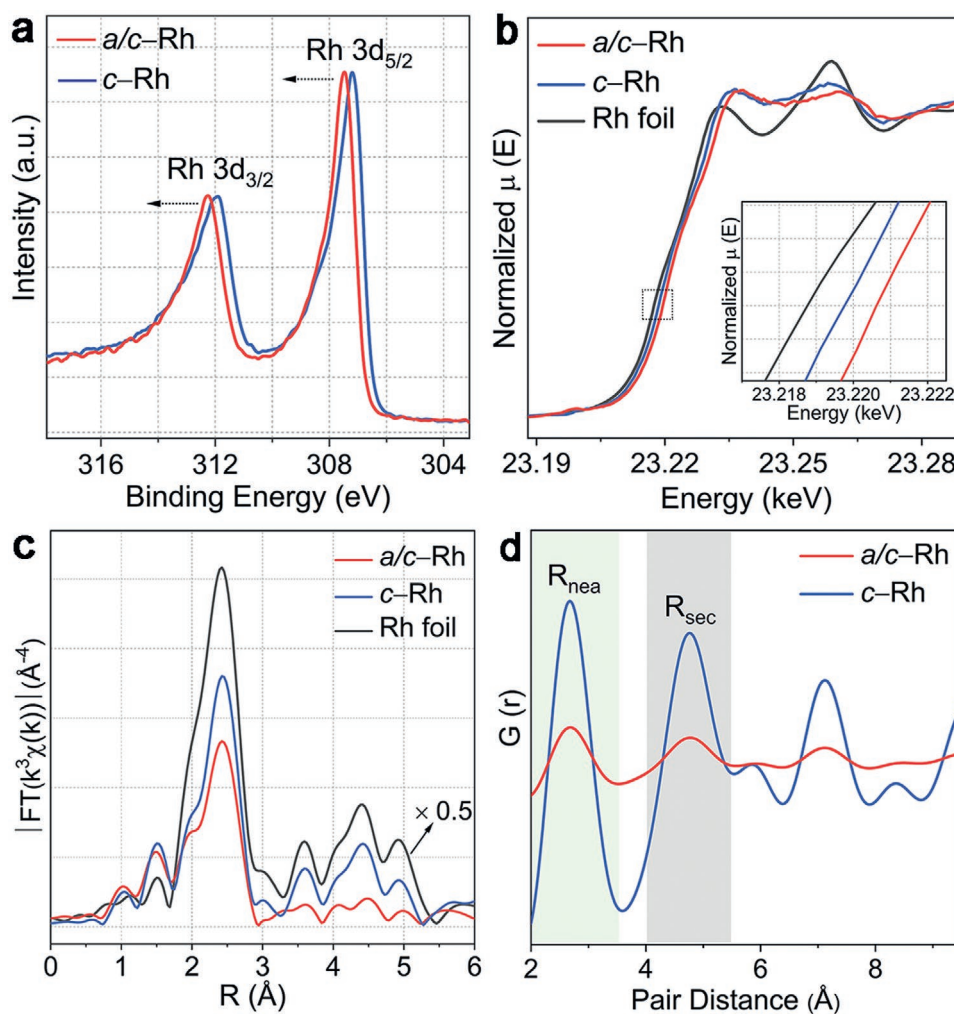


**Figure 2.** Structure analysis of the *a/c*-Rh NSs. a) XPS spectra of *a/c*-Rh NSs and *c*-Rh NSs. b) XANES and c) Fourier-transform EXAFS spectra of *a/c*-Rh NSs, *c*-Rh NSs, and Rh foil. Inset in (b): enlarged XANES spectra of Rh K-edge taken from the black dot square. d) RDF profiles of *a/c*-Rh NSs and *c*-Rh NSs.

near-edge structure (XANES) and extended X-ray absorption fine structure (EXAFS) spectra of Rh K-edge were collected to further investigate the valence state and the atomic structure of the *a/c*-Rh NSs. As shown in Figure 2b, the Rh K-edge XANES spectrum of the *a/c*-Rh NSs displays a similar pattern but slightly higher energy absorption edge as compared to the *c*-Rh NSs and Rh foil, which is consistent with the aforementioned XPS result. The fitting results of EXAFS spectra of Rh K-edge for *a/c*-Rh NSs, *c*-Rh NSs, and Rh foil (Figure S5 and Table S1, Supporting Information) show almost identical peak positions at  $\approx 2.68$  Å, which is assigned to the Rh-Rh metallic bond. Notably, compared with the *c*-Rh NSs, the peak intensity of *a/c*-Rh NSs in the EXAFS spectra is weaker (Figure S5, Supporting Information), and the coordination number of Rh-Rh in the *a/c*-Rh NSs is lower (Table S1, Supporting Information), which can be ascribed to the decreased atomic ordering.<sup>[23,35]</sup> By using the azimuthal average function of the profile analysis of the selected area electron diffraction (PASAD) script in digital micrograph software, the radial distribution function (RDF) profile was obtained to further analyze the local structural characteristics of the *a/c*- and *c*-Rh NSs (Figure 2d). The two peaks ( $R_{\text{nea}}$  and  $R_{\text{sec}}$ ) in the RDF profile represent the average distance of the nearest and the second nearest neighboring Rh atoms, respectively. Although the  $R_{\text{nea}}$  and  $R_{\text{sec}}$  peaks of the *a/c*-Rh NSs at 2.71 and 4.80 Å, respectively, match well with those of *c*-Rh NSs, they are broader and exhibit weaker intensity compared to

those of the crystalline counterpart, further demonstrating their poor crystallinity.<sup>[34]</sup>

To demonstrate the universality of our facile synthetic approach, bimetallic *a/c*-RhM (M = Cu, Zn, Ru) alloy NSs were prepared by simply mixing Rh(acac)<sub>3</sub> and Cu(acac)<sub>2</sub> or Zn(acac)<sub>2</sub> or Ru(acac)<sub>3</sub> precursors, respectively, in the reaction solution (see the Experimental Section in the Supporting Information for experimental details). Figure 3a–c and Figure S6a–c (Supporting Information) show the TEM and SEM images of as-obtained *a/c*-RhCu, RhZn, and RhRu NSs, respectively, indicating their high uniformity and purity. Similar to the *a/c*-Rh NSs, both amorphous and crystalline domains can be observed in the *a/c*-RhM NSs (Figure 3d–f), which were further confirmed by the diffuse ring (Figure 3d<sub>1</sub>–f<sub>1</sub>) and bright spots (Figure 3d<sub>2</sub>–f<sub>2</sub>) in the corresponding FFT patterns, respectively. The weak rings in the SAED patterns further indicate the low degree of crystallinity of the *a/c*-RhM NSs (Figure S7, Supporting Information). Moreover, only weak diffraction peaks at around 40–45° were observed in the XRD patterns of the as-prepared RhM NSs (Figure S8, Supporting Information), indicating their poor crystallinity. The elemental mappings (Figure 3g–i) show the homogeneous distribution of Rh and the alloyed metals in the *a/c*-RhM NSs. By using energy dispersive X-ray spectroscopy (EDX, Figure S9, Supporting Information), the Rh/Cu, Rh/Zn, and Rh/Ru atomic ratios are estimated to be 0.7/0.3, 0.9/0.1, and 0.9/0.1, respectively.

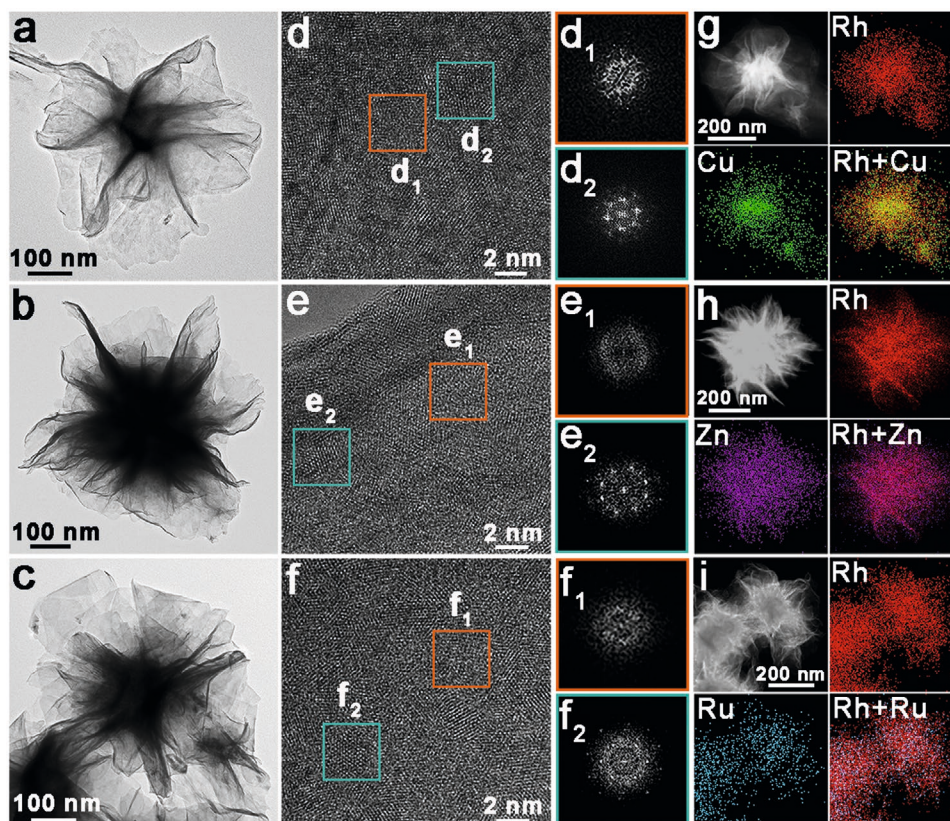


**Figure 3.** Characterization of the bimetallic *a/c*-RhM (M = Cu, Zn, Ru) alloy NSs. a–c) TEM and d–f) aberration-corrected HRTEM images of ultrathin *a/c*-RhCu, RhZn, and RhRu NSs, respectively. d<sub>1</sub>–f<sub>2</sub>) FFT patterns taken from the corresponding orange and cyan square areas in (d–f), respectively. g–i) DF-STEM images and the corresponding STEM–EDS element mappings of *a/c*-RhCu, RhZn, and RhRu NSs, respectively.

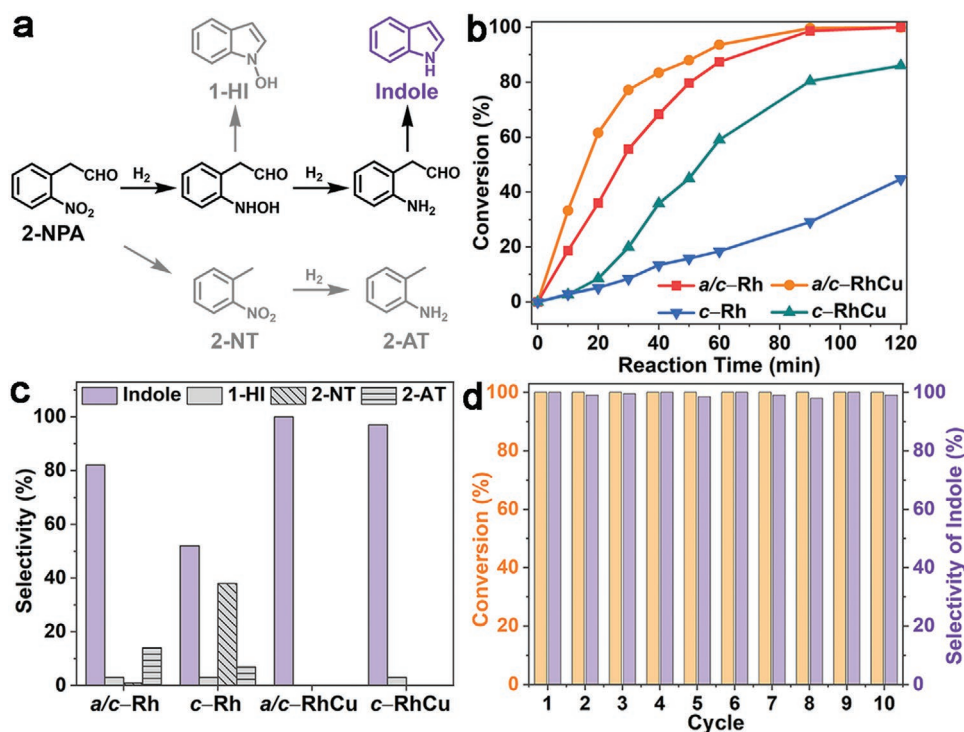


**Figure 4.** Catalytic performances of Rh and RhCu tandem catalysts in the direct synthesis of indole. a) Schematic illustration of the tandem reaction of 2-NPA. Two intermediates in the reaction process are (2-(hydroxyamino)phenyl)acetaldehyde and (2-aminophenyl)acetaldehyde. b) The conversion of 2-NPA and c) the selectivity of products, using *a/c*-Rh, *c*-Rh, *a/c*-RhCu, and *c*-RhCu NSs as catalysts. d) Recycling test of the *a/c*-RhCu NSs. Reaction condition: 2-NPA (0.05 mmol), catalyst (1 mol%), 1 mL of mixed solvent of DMF and H<sub>2</sub>O (*v/v* = 5/1), 1 atm H<sub>2</sub>, 80 °C, and 120 min.

Rh-based materials are promising heterogeneous catalysts for a variety of tandem reactions.<sup>[3,36,37]</sup> As a proof-of-concept application, the catalytic performance of the obtained Rh NSs was investigated in the tandem catalysis for direct indole synthesis via the reduction of nitroarenes to anilines and subsequent aldimine condensation.<sup>[5,38]</sup> The (2-nitrophenyl)acetaldehyde (2-NPA), one kind of nitroarene, was first synthesized (see the Experimental Section in the Supporting Information for experimental details), and then used as the substrate for the tandem reaction (Figure 4a), which was conducted in a Schlenk tube at 80 °C under 1 atm H<sub>2</sub> atmosphere (see the Experimental Section in the Supporting Information for experimental details). After 120 min of reaction, the conversions of 2-NPA catalyzed by the *a/c*-Rh NSs and *c*-Rh NSs are 100% (Figure 4b, red curve) and 45% (Figure 4b, blue curve), respectively, indicating the higher catalytic activity of the *a/c*-Rh NSs compared to the *c*-Rh NSs. As a result, the selectivities of indole are 82% and 52% on the *a/c*-Rh NSs and *c*-Rh NSs, respectively (Figure 4c). Besides indole, by-products, such as 1-hydroxyindole (1-HI), 2-nitrotoluene (2-NT) and 2-aminotoluene (2-AT) shown in grey in Figure 4a were also detected (Figure 4c; Figures S10a,b and S11–S14 and Table S2, Supporting Information). It suggests that more than one pathways took place during the tandem catalytic process (Figure 4a). Therefore, the selectivity of indole is highly desired to be further improved.

Since Cu alloying represents an effective way to enhance the selectivity of noble metal nanocatalysts,<sup>[39–41]</sup> the catalytic performance of the *a/c*-RhCu NSs was further investigated. The *c*-RhCu NSs were also synthesized and used as a catalyst

(Figures S15 and S16, Supporting Information, see the Experimental Section in the Supporting Information for experimental details). Remarkably, the selectivities of indole on the *a/c*-RhCu and *c*-RhCu NSs are improved to >99.9% and 97%, respectively (Figure 4c; Figure S10c,d and Table S2, Supporting Information), much higher than those of *a/c*-Rh NSs (82%) and *c*-Rh NSs (52%). Moreover, by using the *a/c*-RhCu NSs as catalyst, the conversion of 2-NPA reached 100% within 90 min (Figure 4b, orange curve), greater than that using the *a/c*-Rh (98.7%, Figure 4b, red curve) and *c*-RhCu catalysts (80.3%, Figure 4b, cyan curve). The aforementioned results suggest that alloying Cu can simultaneously improve the selectivity and activity of the obtained *a/c*-RhCu NSs. To the best of our knowledge, the overall catalytic performance of the *a/c*-RhCu NSs is superior to the most reported noble-metal-based homogeneous and heterogeneous catalysts toward the indole synthesis (Table S3, Supporting Information). Furthermore, the stability of the *a/c*-RhCu NSs was evaluated by the recycling test. As shown in Figure 4d, the *a/c*-RhCu NSs have been recycled for ten times without significant decay of the catalytic performance. In addition, the morphology and crystallinity of the recycled *a/c*-RhCu NSs catalyst were retained as evidenced by the TEM image and SAED pattern (Figure S17, Supporting Information), illustrating their high stability. Therefore, the *a/c*-RhCu NSs could be used as excellent heterogeneous catalyst for the direct synthesis of indole.

The high activity and selectivity of the *a/c*-RhCu NSs toward the direct synthesis of indole might originate from the unique amorphous/crystalline heterophase structure and the Rh–Cu

interaction, which could affect the tandem catalytic processes as follows. First, the amorphous/crystalline heterophase can offer more abundant active sites. Compared with their crystalline counterparts (Figures S2c and S15c, Supporting Information), the *a/c*-Rh and *a/c*-RhCu NSs possess more abundant phase boundaries (Figures S3 and S18, Supporting Information) which could serve as active sites to boost the hydrogenation rate of the nitro group ( $-\text{NO}_2$ )<sup>[42]</sup> and thus improve the catalytic activity. In addition, the undercoordinated Rh atoms in the amorphous domains, as confirmed by the fitted EXAFS data (Table S1, Supporting Information), could also serve as the active sites for the catalytic reactions, further improving their catalytic activity for hydrogenation process.<sup>[10]</sup> Second, Cu alloying to form RhCu NSs could further accelerate the hydrogenation process. As shown in the XPS spectra (Figure S19, Supporting Information), the Rh 3d<sub>5/2</sub> and 3d<sub>3/2</sub> peaks in the *a/c*-RhCu catalysts shift to more negative value compared to the *a/c*-Rh NSs, indicating the electron donation from Cu to Rh, thus leads to higher electron density of Rh in the *a/c*-RhCu NSs.<sup>[43,44]</sup> The increased electron density of Rh could result in the weaker surface binding of H atoms on Rh atoms<sup>[23,45–47]</sup> further enhancing the hydrogenation activity.<sup>[42,48–50]</sup> Since H<sub>2</sub> only participated in the reduction of unsaturated bonds, when *a/c*-RhCu NSs instead of *a/c*-Rh NSs are used as the catalyst, the hydrogenation step (Figure 4a) 2-NPA to (2-aminophenyl)acetaldehyde) in the tandem reaction could be greatly promoted, and the decarbonylation rate of aldehyde group (Figure 4a) 2-NPA to 2-NT, non-hydrogenation process) would be suppressed. As a result, the obtained amine intermediate, i.e., (2-aminophenyl)acetaldehyde, can be rapidly condensed with the adjacent aldehyde group by the tandem process, leading to the more favored production of indole.

In summary, we have developed a facile and general wet-chemical strategy for the synthesis of ultrathin amorphous/crystalline Rh NSs and bimetallic RhM (M = Cu, Zn, Ru) alloy NSs. The heterophase and alloying of Cu are found to boost the performance of the obtained RhCu NSs as efficient heterogeneous tandem catalysts for the direct indole synthesis. Impressively, with the presence of amorphous-crystalline phase boundaries, the *a/c*-Rh NSs exhibit a higher catalytic activity compared with the *c*-Rh NSs. By further alloying Cu, 100% conversion and >99.9% selectivity of indole are obtained on the formed *a/c*-RhCu NSs. The modified electronic structure in bimetallic RhCu NSs can weaken the interaction between Rh and hydrogen, which could be the reason for the superior selectivity toward indole. Our work demonstrates the importance of phase engineering of nanomaterials (PEN) and metal alloying in the rational design of Rh-based catalysts, providing a new avenue for developing efficient metal nanocatalysts for the fine chemical synthesis.

## Supporting Information

Supporting Information is available from the Wiley Online Library or from the author.

## Acknowledgements

J.G., P.Y., and Y.C. contributed equally to this work. The authors would like to acknowledge the Facility for Analysis, Characterization, Testing,

and Simulation, Nanyang Technological University, Singapore, for use of their electron microscopy (and/or X-ray) facilities. H.Z. thanks the support from ITC via Hong Kong Branch of National Precious Metals Material Engineering Research Center (NPMM), the Start-Up Grant (Project No. 9380100) and grants (Project Nos. 9610478 and 1886921) from City University of Hong Kong.

## Conflict of Interest

The authors declare no conflict of interest.

## Keywords

amorphous structures, heterophases, indole synthesis, Rh and Rh alloys, tandem catalysis, ultrathin nanosheets

Received: October 4, 2020

Revised: December 9, 2020

Published online: January 25, 2021

- [1] G. W. Gribble, *Indole Ring Synthesis: From Natural Products to Drug Discovery*, John Wiley & Sons Ltd., Chichester, UK 2016.
- [2] M. Inman, C. J. Moody, *Chem. Sci.* **2013**, 4, 29.
- [3] C. Xie, Z. Niu, D. Kim, M. Li, P. Yang, *Chem. Rev.* **2019**, 120, 1184.
- [4] Z. Xu, Q. Wang, J. Zhu, *J. Am. Chem. Soc.* **2013**, 135, 19127.
- [5] Y. Zhao, H. Zhou, W. Chen, Y. Tong, C. Zhao, Y. Lin, Z. Jiang, Q. Zhang, Z. Xue, W.-C. Cheong, B. Jin, F. Zhou, W. Wang, M. Chen, X. Hong, J. Dong, S. Wei, Y. Li, Y. Wu, *J. Am. Chem. Soc.* **2019**, 141, 10590.
- [6] X.-Y. Liu, Y. Qin, *Acc. Chem. Res.* **2019**, 52, 1877.
- [7] R. Mancuso, R. Dalpozzo, *Catalysts* **2018**, 8, 458.
- [8] D. R. Stuart, M. Bertrand-Laperle, K. M. N. Burgess, K. Fagnou, *J. Am. Chem. Soc.* **2008**, 130, 16474.
- [9] Y. Shang, K. Jonnada, S. L. Yedage, H. Tu, X. Zhang, X. Lou, S. Huang, W. Su, *Chem. Commun.* **2019**, 55, 9547.
- [10] H. Duan, N. Yan, R. Yu, C.-R. Chang, G. Zhou, H.-S. Hu, H. Rong, Z. Niu, J. Mao, H. Asakura, T. Tanaka, P. J. Dyson, J. Li, Y. Li, *Nat. Commun.* **2014**, 5, 3093.
- [11] X. Fu, Z. Zhao, C. Wan, Y. Wang, Z. Fan, F. Song, B. Cao, M. Li, W. Xue, Y. Huang, X. Duan, *Nano Res.* **2019**, 12, 211.
- [12] R. Lang, T. Li, D. Matsumura, S. Miao, Y. Ren, Y.-T. Cui, Y. Tan, B. Qiao, L. Li, A. Wang, X. Wang, T. Zhang, *Angew. Chem., Int. Ed.* **2016**, 55, 16054.
- [13] B. L. Tran, J. L. Fulton, J. C. Linehan, J. A. Lercher, R. M. Bullock, *ACS Catal.* **2018**, 8, 8441.
- [14] C. Gao, J. Wang, H. Xu, Y. Xiong, *Chem. Soc. Rev.* **2017**, 46, 2799.
- [15] X. Cui, W. Li, P. Ryabchuk, K. Junge, M. Beller, *Nat. Catal.* **2018**, 1, 385.
- [16] Y. Wang, L. Zhang, C. Hu, S. Yu, P. Yang, D. Cheng, Z.-J. Zhao, J. Gong, *Nano Res.* **2019**, 12, 2268.
- [17] Y. Chen, Z. Lai, X. Zhang, Z. Fan, Q. He, C. Tan, H. Zhang, *Nat. Rev. Chem.* **2020**, 4, 243.
- [18] M. Zhou, T. Higaki, G. Hu, M. Y. Sfeir, Y. Chen, D.-e. Jiang, R. Jin, *Science* **2019**, 364, eaaw9545.
- [19] H. Cheng, N. Yang, Q. Lu, Z. Zhang, H. Zhang, *Adv. Mater.* **2018**, 30, 1707189.
- [20] Z. Fan, Z. Luo, X. Huang, B. Li, Y. Chen, J. Wang, Y. Hu, H. Zhang, *J. Am. Chem. Soc.* **2016**, 138, 1414.
- [21] Q. Lu, A.-L. Wang, Y. Gong, W. Hao, H. Cheng, J. Chen, B. Li, N. Yang, W. Niu, J. Wang, Y. Yu, X. Zhang, Y. Chen, Z. Fan, X.-J. Wu, J. Chen, J. Luo, S. Li, L. Gu, H. Zhang, *Nat. Chem.* **2018**, 10, 456.

- [22] P.-F. Yin, M. Zhou, J. Chen, C. Tan, G. Liu, Q. Ma, Q. Yun, X. Zhang, H. Cheng, Q. Lu, B. Chen, Y. Chen, Z. Zhang, J. Huang, D. Hu, J. Wang, Q. Liu, Z. Luo, Z. Liu, Y. Ge, X.-J. Wu, X.-W. Du, H. Zhang, *Adv. Mater.* **2020**, *32*, 2000482.
- [23] N. Yang, H. Cheng, X. Liu, Q. Yun, Y. Chen, B. Li, B. Chen, Z. Zhang, X. Chen, Q. Lu, J. Huang, Y. Huang, Y. Zong, Y. Yang, L. Gu, H. Zhang, *Adv. Mater.* **2018**, *30*, 1803234.
- [24] H. Han, H. Choi, S. Mhin, Y.-R. Hong, K. M. Kim, J. Kwon, G. Ali, K. Y. Chung, M. Je, H. N. Umh, D.-H. Lim, K. Davey, S.-Z. Qiao, U. Paik, T. Song, *Energy Environ. Sci.* **2019**, *12*, 2443.
- [25] H. Cheng, N. Yang, X. Liu, Q. Yun, M. H. Goh, B. Chen, X. Qi, Q. Lu, X. Chen, W. Liu, L. Gu, H. Zhang, *Natl. Sci. Rev.* **2019**, *6*, 955.
- [26] Y. Yao, S. Hu, W. Chen, Z.-Q. Huang, W. Wei, T. Yao, R. Liu, K. Zang, X. Wang, G. Wu, W. Yuan, T. Yuan, B. Zhu, W. Liu, Z. Li, D. He, Z. Xue, Y. Wang, X. Zheng, J. Dong, C.-R. Chang, Y. Chen, X. Hong, J. Luo, S. Wei, W.-X. Li, P. Strasser, Y. Wu, Y. Li, *Nat. Catal.* **2019**, *2*, 304.
- [27] C. H. Wu, C. Liu, D. Su, H. L. Xin, H.-T. Fang, B. Eren, S. Zhang, C. B. Murray, M. B. Salmeron, *Nat. Catal.* **2019**, *2*, 78.
- [28] K. D. Gilroy, A. Ruditskiy, H.-C. Peng, D. Qin, Y. Xia, *Chem. Rev.* **2016**, *116*, 10414.
- [29] J. Mao, W. Chen, W. Sun, Z. Chen, J. Pei, D. He, C. Lv, D. Wang, Y. Li, *Angew. Chem., Int. Ed.* **2017**, *56*, 11971.
- [30] J. Mao, C.-T. He, J. Pei, W. Chen, D. He, Y. He, Z. Zhuang, C. Chen, Q. Peng, D. Wang, Y. Li, *Nat. Commun.* **2018**, *9*, 4958.
- [31] Y. Jiang, J. Su, Y. Yang, Y. Jia, Q. Chen, Z. Xie, L. Zheng, *Nano Res.* **2016**, *9*, 849.
- [32] Y. Zhao, S. Xing, X. Meng, J. Zeng, S. Yin, X. Li, Y. Chen, *Nanoscale* **2019**, *11*, 9319.
- [33] H. Cheng, N. Yang, G. Liu, Y. Ge, J. Huang, Q. Yun, Y. Du, C.-J. Sun, B. Chen, J. Liu, H. Zhang, *Adv. Mater.* **2020**, *32*, 1902964.
- [34] G. Wu, X. Zheng, P. Cui, H. Jiang, X. Wang, Y. Qu, W. Chen, Y. Lin, H. Li, X. Han, Y. Hu, P. Liu, Q. Zhang, J. Ge, Y. Yao, R. Sun, Y. Wu, L. Gu, X. Hong, Y. Li, *Nat. Commun.* **2019**, *10*, 4855.
- [35] A. I. Frenkel, C. W. Hills, R. G. Nuzzo, *J. Phys. Chem. B* **2001**, *105*, 12689.
- [36] R. Liu, R. Jin, J. An, Q. Zhao, T. Cheng, G. Liu, *Chem. Asian J.* **2014**, *9*, 1388.
- [37] J. Lu, J. Dimroth, M. Weck, *J. Am. Chem. Soc.* **2015**, *137*, 12984.
- [38] Y. Yamane, X. Liu, A. Hamasaki, T. Ishida, M. Haruta, T. Yokoyama, M. Tokunaga, *Org. Lett.* **2009**, *11*, 5162.
- [39] Q. Yang, R. Hou, K. Sun, *J. Catal.* **2019**, *374*, 12.
- [40] O. B. Ayodele, R. Cai, J. Wang, Y. Ziouani, Z. Liang, M. C. Spadaro, K. Kovnir, J. Arbiol, J. Akola, R. E. Palmer, Y. V. Kolen'ko, *ACS Catal.* **2019**, *10*, 451.
- [41] R. Long, Y. Li, Y. Liu, S. Chen, X. Zheng, C. Gao, C. He, N. Chen, Z. Qi, L. Song, J. Jiang, J. Zhu, Y. Xiong, *J. Am. Chem. Soc.* **2017**, *139*, 4486.
- [42] Y. Wang, R. Qin, Y. Wang, J. Ren, W. Zhou, L. Li, J. Ming, W. Zhang, G. Fu, N. Zheng, *Angew. Chem., Int. Ed.* **2020**, *59*, 12736.
- [43] M. Mateen, K. Shah, Z. Chen, C. Chen, Y. Li, *Nano Res.* **2019**, *12*, 1631.
- [44] D. Cao, H. Xu, D. Cheng, *Adv. Energy Mater.* **2020**, *10*, 1903038.
- [45] J. Greeley, M. Mavrikakis, *J. Phys. Chem. B* **2005**, *109*, 3460.
- [46] G. Giannakakis, M. Flytzani-Stephanopoulos, E. C. H. Sykes, *Acc. Chem. Res.* **2019**, *52*, 237.
- [47] M. Zhao, K. Yuan, Y. Wang, G. Li, J. Guo, L. Gu, W. Hu, H. Zhao, Z. Tang, *Nature* **2016**, *539*, 76.
- [48] S. Furukawa, Y. Yoshida, T. Komatsu, *ACS Catal.* **2014**, *4*, 1441.
- [49] S. Cai, H. Duan, H. Rong, D. Wang, L. Li, W. He, Y. Li, *ACS Catal.* **2013**, *3*, 608.
- [50] L. Wang, E. Guan, J. Zhang, J. Yang, Y. Zhu, Y. Han, M. Yang, C. Cen, G. Fu, B. C. Gates, F.-S. Xiao, *Nat. Commun.* **2018**, *9*, 1362.